Hygrothermal properties of an early 20th century clay brick from eastern France: Experimental characterization and numerical modelling

Yacine Ait Oumeziane, Alexandre Pierre, Fatima El Mankibi, Valérie Lepiller, Marina Gasnier, Philippe Désévaux

Hygrothermal properties of an early 20th century clay brick from eastern France: experimental characterization and numerical modelling

Authors

Aït Oumeziane Yacine[1*], Pierre Alexandre[2], El Mankibi Fatima[1], Lepiller Valérie[1], Gasnier Marina[3], Désévaux Philippe[1]

[1] FEMTO-ST Institute, CNRS 6174, Univ. Bourgogne Franche-Comte, 2 avenue Jean Moulin, 90000 Belfort, France

[2] Laboratoire de Mécanique & Matériaux du Génie Civil, EA 4114, University of Cergy-Pontoise, 5 mail Gay-Lussac,95000 Cergy-Pontoise, France

[3] FEMTO-ST Institute/RECITS, CNRS 6174, Univ. Bourgogne Franche-Comte, 2 avenue Jean Moulin, 90000 Belfort, France

[*] Corresponding author: Aït Oumeziane Yacine, yacine.ait_oumeziane@univ-fcomte.fr, +33 (0)3 84 58 76 25, FEMTO-ST Institute, CNRS 6174, Univ. Bourgogne Franche-Comte, 2 avenue Jean Moulin, 90000 Belfort, France

Highlights

- The hygrothermal properties of an early 20th century clay brick are experimentally characterized.
- The measured properties show the interesting hygrothermal performance of the material.
- The temperature-dependent sorption mechanisms are characterized and modelled.

Abstract

This paper deals with the experimental hygrothermal characterization of an early 20th century clay brick, representative of historical industrial buildings in eastern France. The renovation and adaptive reuse of industrial heritage buildings require accurate knowledge of the properties of these existing buildings envelopes, for which few data are available in literature. Hence, for example, the application of the French Thermal Regulation to existing old buildings can lead to unexpected damages, like brick spalling due to freeze-thaw phenomenon if a poorly suited additional interior insulation layer is installed. Despite its hygrothermal advantages, external insulation must be avoided for aesthetic and historical values of heritage buildings and it is often prohibited by city codes or historic building preservation regulations. In this context and as literature is scarce, it is relevant to deepen the knowledge of this ancient material in order to better understand the hygrothermal behaviour of old industrial buildings to better preserve them. As a first step towards this goal, the main objective of this paper is to give new data about the hygrothermal properties of an early 20th century brick from eastern France. A comparison between models and measured experimental data is also proposed. In particular, the temperature-dependent hysteretic sorption phenomenon, which occurs in brick, is experimentally and numerically investigated.

Keywords: industrial heritage, ancient brick, hygrothermal properties, sorption mechanism

1. Introduction

The global context of sustainable development forces builders to conjointly think about energy consumption and carbon footprint reduction, hygrothermal comfort and indoor air quality for the occupants. Both in France and in Europe, the building sector represents more than 40% of energy consumption and about 25% of CO_2 emission [1, 2]. Energy efficiency of existing buildings is crucial to mitigate climate change. Industrial heritage buildings have a high potential for renovation or adaptive reuse [3-4], which can conserve embodied energy and therefore lower the impact of construction [5-7].

In order to enhance this heritage, historical buildings and materials have hygrothermal performance which deserves to be analysed [8, 9]. For illustration, four examples of industrial sites and buildings are presented in Figure 1.

Figure 1 Examples of industrial sites and buildings: in eastern France a) and b) Techn'hom – business development zone, adaptive reuse of the old spinning factory Dollfus, Mieg & Cie (Belfort, France), b) currently: General Electric European headquarter © Marina Gasnier, 2016 (architect: Reichen and Robert); c) Adaptive reuse of the Le Blan-Lafont textile factory in an urban activities area dedicated to information and communication technologies (architect: Vincent Brossy). In the foreground: the water garden, an element of

stormwater runoff management (Lille, France) © Marina Gasnier, 2012; d) University Institute of Architecture – revitalized warehouses (Venice, Italy) © Marina Gasnier, 2013.

However, both in France [10, 11] and abroad [12], current energy regulations are not suited for existing heritage buildings due to a lack of knowledge about their architecture and hygrothermal performance. The 2012 French Thermal Regulation (FTR), based on the previous 2005 version, applied to existing buildings built before 1948, mandates a renovation that can be described as a prescriptive approach "system by system". It means that when the building owner decides to change or install a building system (insulation, heating equipment, ventilation equipment, glazing…), the installed products must meet minimum required efficiency given by the ministerial ruling published the 3rd May 2007, updated the 22th March 2017 and applied since the 1st January 2018.
Some examples of old buildings which were energy retrofitted are available in literature. As explained in Johansson et al. [13], Johansson has monitored four old buildings in Sweden with additional external insulation layer of glass wool protected by a layer of render or a ventilated facade board [14]. Overall, the author observed an improvement of the thermal performance of the walls. In the same way, Capener et al. have also investigated a brick-based building in Sweden retrofitted with 5 cm of external glass wool insulation and two layers of external render [15]. Their measurements showed a 27% reduction in energy use for both heating and domestic hot water, and a reduction of the moisture content in the walls. The main advantage of adding external insulation is that the existing buildings ambiances are kept in warm and dry conditions, the interior space for the occupants remain identical and the thermal bridges are limited.

Nevertheless, to preserve the exterior aesthetic and historical value of heritage buildings, exterior insulation is often prohibited and interior insulation is used to improve the thermal resistance of the walls. Some works were performed to investigate masonry walls retrofitted with an interior insulation [16-18] and with or without vapor barriers [18-20] to evaluate the interest of these solutions to improve the hygrothermal performance of existing walls. Some examples of buildings with brick walls which were energy retrofitted can also be found in literature [21, 22]. These studies show the interest to add an interior insulation to reduce the energy consumption of old brick buildings. Even though this kind of solution improves the thermal performance of the building envelope, it may induce freeze-thaw damage, like brick spalling. Indeed, the exterior side of the wall gets colder and water can condense within the masonry, which can sometimes initiate freeze-thaw damage [16, 23, 24]. Some procedures to evaluate this risk are proposed in [16, 23, 24].

As underlined by Guizzardi et al. [25], moisture is known to be one of the main origins of damages in building facades and wind-driven rain can be considered as a main external moisture source for exterior walls [26, 27].

According to De Mates et al., in order to bring some solutions to address these issues, capillary active insulation systems are often promoted [28]. These systems are based on a vapour permeable and hygroscopic insulation material, which prevents internal condensation by adsorbing and desorbing moisture depending on outdoor and indoor climatic variations [29]. Grunewald et al. showed the advantages of these materials for historical buildings with thick masonry walls [30].

Johansson et al. [13], Ait Oumeziane et al. [18] and Guzzardi et al. [25] led some experimental campaigns in order to analyze the hygrothermal performance of masonry envelopes of heritage buildings respectively with an interior insulation layer of vacuum insulation panels, with different insulation materials (wood wool, glass wool…) and with a highly insulating render. For information, vacuum insulation panels are highly efficient thermal insulation materials which present the advantage to increase the thermal resistance of a wall compared to conventional insulation materials with a lower thickness.

Harrestrup and Svendsen led an experimental campaign to retrofit an old building in Denmark. In order to preserve the original architectural character of the building, an internal insulation was chosen. In their study, the solution is to end insulation 20 cm above the floor [31]. They showed that no risk of moisture damage occurs in the wooden beams-ends embedded in the masonry brick wall and that the measured energy consumption was reduced by 47% [31].

All these measurements are usually dedicated to be implemented in numerical models that are currently used in building physics to evaluate the hygrothermal performance of a wall. For example, Johansson et al. [13] and Jamal et al. [32] have numerically evaluated the influence of interior insulation on the hygrothermal response of brick masonry walls subjected to climatic variations. In their work, Harrestrup and Svendsen observed that the simulated evolution of temperature and heat flow in the wall are consistent with experimental results [31]. Nevertheless, some discrepancies between experimental and numerical results are observed for the relative humidity evolution inside the walls [13, 18]. This paper's aim is to take a step back and study the hygrothermal properties of the ancient brick first in order to reduce those discrepancies.

Furthermore, in masonry walls, the bricks are joined using mortar. The influence of the mortar has been studied by Vereeken et al. in [33] and later by Zhou et al. in [34]. As shown by Vereeken et al., the assumption to consider the whole wall as a homogenous brick layer is allowed [33]. Furthermore, as highlighted by Zhou et al.

in [34], moisture transport in masonry walls may be affected by the interface resistance, especially when this interface is close to a moisture source. The authors showed that the orientation of the interface, either horizontal or vertical, between brick and mortar does not have an influence on the value of the interface resistance. However, they underlined that the interface resistance depends on the capillary pressure at the interface. Therefore, studying the brick material is relevant as it is the primary driver of the hygrothermal behaviour of the whole building envelope.

However, data for old bricks are very scarce in literature and this current lack of knowledge of heritage industrial architecture and materials behaviour may lead to discrepancies between experimental and numerical simulation results [13, 18] and sometimes lead to irreversible consequences in terms of heritage preservation and damages [11, 23, 24].

In order to preserve the industrial buildings heritage, it appears necessary to extend our knowledge about the hygrothermal behaviour of such buildings, starting by its principal component, the brick.
Experimental hygrothermal characterisation works of modern clay brick are available in literature [35-37]. Indeed, its use in the building construction sector is widespread. Clay bricks are formed by mechanical dry-pressing, molding or extrusion of the clay to give bricks the required dimensions and shape [38]. The 2012 French Thermal Regulation gives reference values. The thermal conductivity ranges from 0.34 $W.m^{-1}.K^{-1}$ for lightweight clay bricks with a dry bulk density under 1000 $kg.m^{-3}$ to 1.04 $W.m^{-1}.K^{-1}$ for heavyweight bricks with a dry bulk density between 2300 and 2400 $kg.m^{-3}$. The specific heat is determined to be 1000 $J.kg^{-1}.K^{-1}$ and the vapour diffusion resistance factor ranges from 16 in dry state to 10 in wet state [39].

The research on the hygrothermal characterisation of historical materials, especially for old bricks, remains less advanced. Engineers and researchers usually use existing materials database, like the Wufi database for example [40], to evaluate the hygrothermal response of a brick wall to climatic variations. To the knowledge of the authors, the available data for old bricks are:

- the “Vienna 1900s brick” which is a brick produced in the 1900s in Vienna [40],
- the “Historical manufactured brick” which is a new brick produced using old manufacturing process [40]. This handcrafted brick, fired in a circular kiln, has been made for restoration purpose by the old Falkenlöwe company. Its properties are similar to those of original medieval bricks in terms of density, porosity, pore size distribution and capillary suction [41].

- Furthermore, Johansson et al. [13] have also experimentally determined some hygrothermal properties of a brick built in a laboratory according to the traditional methods used from the end of the nineteenth century to the early twentieth century in Sweden and Norway. In this paper, this brick is called "Nordic 1900s brick".

Their main hygrothermal properties are presented in Table 1 with ρ_0 (kg.m^{-3}) the dry bulk density, ρ_s (kg.m^{-3}) the solid matrix density, n_0 (%) the open porosity, u_{sat} (%) the saturated moisture content, λ_0 (W.m^{-1}.K^{-1}) the dry thermal conductivity, c_{p0} (J.kg^{-1}.K^{-1}) the dry specific heat, μ_0 (-) the vapour diffusion resistance factor in dry state and D_{ws} (m^2.s^{-1}) the liquid water transport coefficient at saturation. The comparison of the sorption isotherms of different bricks will be discussed later in the paper.

	ρ_0 (kg.m^{-3})	ρ_s (kg.m^{-3})	n_0 (%)	u_{sat} (%)	λ_0 (W.m^{-1}.K^{-1})	c_{p0} (J.kg^{-1}.K^{-1})	μ_0 (-)	D_{ws} (10^{-6} m^2.s^{-1})
Vienna 1900s brick" [40]	1560	2516	38	24	0.6	850	15	17
"Historical manufactured brick" [40]	1780	2580	32	18	0.6	850	9.5	8.9
"Nordic 1900s brick"[13]	1810	-	-	-	-	-	-	2.4

Table 1 Hygrothermal properties of three historical clay bricks

These three bricks have different physical and hygric properties and may present different hygrothermal responses to climatic variations.

In this context, the objective of this paper is to experimentally characterize the hygrothermal properties of an early 20th century clay brick representative of old industrial buildings in eastern France in order to enrich the current database on historical materials. The studied properties are bulk and absolute densities, open porosity,

water vapour permeability, liquid water transport coefficient, specific heat and thermal conductivity. The measured experimental data are then compared to theoretical models.

Moreover, it has been demonstrated in literature [42, 43] that moisture content is the most sensitive parameter that governs at the first order the evolution of the hygrothermal properties and transfer through a wall.

Due to the hysteretic effect, the equilibrium moisture content depends not only on relative humidity but also on moisture variations undergone by the material. The temperature also influences the equilibrium moisture content. The hysteresis phenomenon and temperature effects on the sorption process are most very often neglected when modelling the moisture content evolution in heat and moisture transfer models. This can cause significant discrepancies to predict the hygrothermal response of a material subjected to climatic variations [44, 45]. Therefore, a special attention is paid in this study to the moisture content evaluation. Thus, the hysteresis phenomenon and the thermo-dependent sorption mechanism are experimentally characterized. To the knowledge of the authors, similar studies for ancient brick masonry are not available.

2. Materials and Methods

2.1. Materials

The bricks were used for the construction of industrial buildings in the eastern region of France mainly dedicated to the spinning activities at the early twentieth century (Figure 1a and Figure 1b). They came from an industrial brickyard (Oscar Lesage) founded in 1897 and located in the neighbourhood of Mulhouse in eastern France (former spinning factory Dollfus, Mieg and Cie). An archival research uncovered to find two technical reports drafted in 1936 by the "Laboratoire officiel du Syndicat des fabricants de produits céramiques de France" [47] and in 1952 [46]. These documents are a precious source of information for the chemical composition of historical bricks. It specifies that the bricks are made with about 60% of red earth and 40% of Burhaupt yellow earth. For further information, the chemical composition of the red earth is detailed in Table 2. The report also specifies also the operating process. The samples were first oven-dried at 100-110°C. Then, they were analysed by usual methods after alkali carbonates and chloric acid attacks until fully evaporation [46].

silica	titanium dioxide	alumina	iron sesquioxide	lime	magnesia	sulphur trioxide	alkali	carbon dioxide	complementary ignition loss
62.35	0.50	19.15	7.10	1.10	0.15	0.75	3.60	0.45	4.95

Table 2 Chemical composition of the red earth (in %)

Table 2 shows that the red earth is poor in lime with a high silica rate. An analogous analysis performed on yellow earth gives a low lime rate and suited silica, alumina and iron rates to the brick masonry [47].

Figure 2 a. presents the set of the studied bricks collected in Mulhouse in eastern France. The samples are taken from the same location during demolition works and come from a same building. It should be highlighted that the samples collection on site is particularly complex because of the patrimonial value of the industrial buildings. Renovation projects or demolition works remain the only opportunities to collect samples.

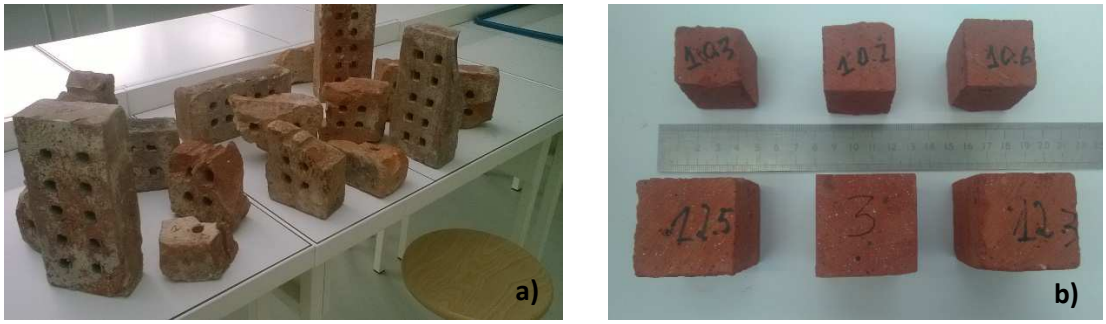

Figure 2 Raw perforated clay bricks a) and samples b) from the former spinning factory Dollfus, Mieg and Cie - bricks dating back to the 1920's

The dimensions of the raw perforated bricks are 25 × 12 × 6 cm^3. The dimensions of the samples are constrained by the holes in the perforated bricks. Different types of samples were prepared for the study: 6 × 12 × 2.5 cm^3 for measuring water vapour permeability and liquid water transport coefficient at saturation, 4 × 4 × 4 cm^3 and 3 × 3 × 3 cm^3 for measuring the sorption isotherms. The samples for measuring the specific heat and the thermal conductivity are 6 × 4 × 2 cm^3.

2.2. Methods

2.2.1. Physical characterisation

To verify if the volume of the samples is superior to the Representative Elementary Volume (REV), the raw bricks dry bulk densities are first measured. According to the NF EN ISO 12570 [48], the bricks are dried to constant weight in a ventilated oven at 105°C until steady state reached when the mass variation for 3 consecutive measurements during 24 hours is less than 0.1%.

The shape of the raw perforated bricks is irregular (Figure 2). The hydrostatic weighing method is thus used according to the standard NF EN 772-3 [49] for the raw bricks and according to NF EN 772-4 [50] for the

samples. The dry bulk density is determined from the mass of the dry sample m_0 [kg], the mass of the water-saturated sample $m_{air,sat}$ [kg] in air and the mass of the immersed water-saturated sample $m_{imm,sat}$ [kg]:

$$\rho_0 = \rho_w \frac{m_0}{m_{air,sat} - m_{imm,sat}} \quad (1)$$

with ρ_w [kg.m^{-3}] the water density. A 10-kg Kern PCB 10000-1 balance (accuracy 10^{-1} g) is used for the raw bricks and a 520-g VWR LPW-503i balance (accuracy 10^{-3} g) for the samples.

The saturated mass moisture content u_{sat} [kg.kg^{-1}] is determined from Eq. 2.

$$u_{sat} = \frac{m_{air,sat} - m_0}{m_0} \quad (2)$$

The open porosity n_0 [-] is deduced from Eq.2 by the relation:

$$n_0 = \frac{u_{sat}\rho_0}{\rho_w} \quad (3)$$

The solid matrix density ρ_s [kg.m^{-3}] is determined from Eq. 4.

$$\rho_s = \frac{\rho_0}{1 - n_0} \quad (4)$$

The dry bulk density of the prismatic samples is also determined with the 520-g VWR LPW-503i balance (accuracy 10^{-3} g) and a calliper (accuracy 10^{-1} mm) for verification.

The volume of the sample is assumed to be representative if the conditions expressed in Eqs. 5 and 6 are satisfied:

$$\frac{\left|\rho_{0,average} - \rho_{0,average,ref}\right|}{\rho_{0,average,ref}} < 5\% \quad (5)$$

$$\frac{\sigma}{\rho_{0,average}} < 10\% \quad (6)$$

$\rho_{0,average}$ [kg.m^{-3}] stands for the average dry bulk density of a set of samples and $\rho_{0,average,ref}$ [kg.m^{-3}] for the average dry bulk density of the raw perforated bricks. The variation coefficient is defined by the rate between the standard variation σ [kg.m^{-3}] and the average dry bulk density of a set of samples.

2.2.2. Hygric characterisation

The adsorption and desorption isotherms are determined according to the requirements of the standard NF EN ISO 12571 [51]. The adsorption isotherm is determined at 23°C from the dry state for four relative humidity levels: 40, 60, 80 and 90% RH in a climatic chamber. The adsorption and desorption isotherms respectively at

10°C and 40°C are determined with the method of saturated salt solutions. The desiccators containing the different solutions are placed in a ± 1°C controlled-temperature room. The different salt solutions and the corresponding generated equilibrium relative humidity are presented in Table 3. The samples are periodically weighed until the difference between three consecutive measurements during 24 h is less than 0.1%.

The mass moisture content u [kg.kg^{-1}] is determined from Eq. 7.

$$u = \frac{m - m_0}{m_0} \tag{7}$$

m [kg] stands for the wet mass of the sample.

Temperature	**Equilibrium relative humidity**				
	sodium acetate	magnesium nitrate	sodium bromide	potassium bromide	potassium sulphate
10°C	23%		60%	83%	98%
23°C		53%			97%
40°C	20%		52%	79%	96%

Table 3 Salts used in desiccators and their equilibrium relative humidity at 10°C, 23°C and 40°C

The vapour permeability is measured as specified in standard NF EN ISO 12572 [52]. The test involves sealing a sample above a test cup containing a saline solution able to set a chosen relative humidity RH_i. The sample is subjected to another relative humidity RH_e on its opposite surface. The system cup / sample is placed in a temperature-controlled chamber where a fan ensures the air circulation above the superior surface. The sealing of the samples ensures the monodimensionnal transfer. The diagram of the experimental device is given in Figure 3.

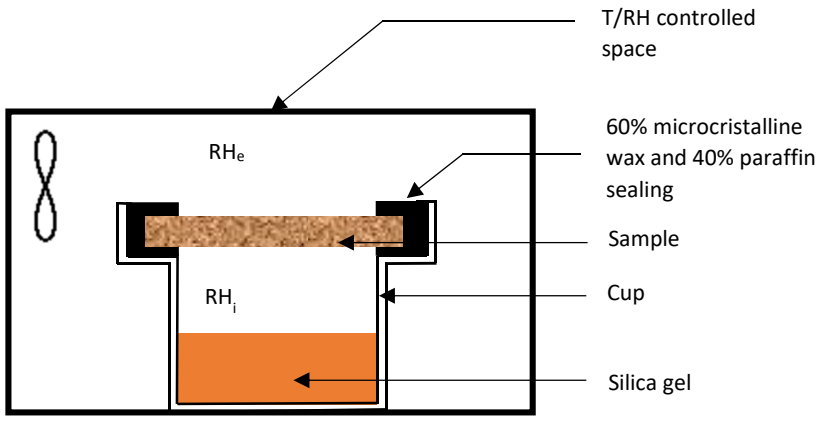

Figure 3 Principle diagram of the cup test method

At the reference temperature of 23°C, the relative humidity difference creates a vapour partial pressure gradient, driving force of the vapour flow through the thickness of the sample. The vapour density g_v [kg.m^{-2}.s^{-1}] is expressed in Eq. 8.

$$g_v = \frac{\delta_p \Delta p_v}{e} \tag{8}$$

δ_p [kg.m^{-1}.s^{-1}.Pa^{-1}] is the vapour permeability of the material, p_v [Pa] the vapour pressure and e [m] the thickness of the sample.

The determination of the vapour flow is based on the mass monitoring of the cup/sample system in function of time. The vapour flow density can thus be also expressed by Eq. 9.

$$g_v = \frac{\frac{\Delta m}{\Delta t}}{S} \tag{9}$$

Δm [kg] is the mass variation of the system during the time period Δt [s] and S [m^2] is the average of the interior and exterior exposed surfaces. Finally, the air gap corrected vapour permeability is deduced in steady state from the relation:

$$\delta_p = \frac{e}{\left[\frac{S\Delta p_v}{\frac{\Delta m}{\Delta t}} - \frac{e_{air}}{\delta_{p,a}}\right]} \tag{10}$$

with e_{air} [m] the air layer thickness between the silica gel and the inferior surface of the sample and $\delta_{p,a}$ [kg.m^{-1}.s^{-1}.Pa^{-1}] the vapour permeability of air.

$$\delta_{p,a} = 2.31\ 10^{-5} \frac{M_l}{RT} \left(\frac{T}{273.15}\right)^{1.81} \tag{11}$$

M_l [18 g.mol^{-1}] is the water molar mass and R is the perfect gas constant [8.314 J.mol^{-1}.K^{-1}].

The determination of the vapour diffusion resistance factor is given by Eq. 12:

$$\mu = \frac{\delta_{p,a}}{\delta_p} \tag{12}$$

The liquid water absorption coefficient A_w [kg.m^{-2}.s$^{-0.5}$] is determined according to NF EN 15148 [53] from the evolution of the water mass in the sample in function of time. The evolution of the liquid transport coefficient D_w [m^2.s^{-1}] is defined by Eq. (13) [54].

$$D_w = 3.8 \left(\frac{A_w}{\rho_0 u_{sat}}\right)^2 1000^{\frac{u}{u_{sat}}-1} \tag{13}$$

u_{sat} [kg.kg^{-1}] is the moisture content at saturation.

The isothermal total diffusion coefficient D_t [m^2.s^{-1}] is the sum of the vapour diffusion coefficient D_v [m^2.s^{-1}] and the liquid diffusion coefficient D_w.

$$\mathrm{D_t} = \mathrm{D_v} + \mathrm{D_w} = \frac{\delta_p p_{sat}(T)}{\rho_0 \frac{\partial u}{\partial RH}} + \mathrm{D_w} \tag{14}$$

2.2.3. Thermal characterisation

The thermal properties of the brick are determined with a Hot Disk probe TPS1500. The Hot Disk method is a fast and accurate transient plane source technique [55, 56]. The principle of the method is to deliver a small constant current during a short time to increase the temperature of the material by a few degrees. This temperature increase depends on the thermal transport properties of the material surrounding the sensor. By monitoring this temperature increase over a short period after the start of the experiment, it is possible to obtain the equivalent thermal conductivity and the thermal diffusivity expressed in Eq. 15:

$$\alpha = \frac{\lambda^*}{\rho c_p^*} \tag{15}$$

In this relation, λ^* [W.m^{-1}.K^{-1}] and c_p^* [J.kg^{-1}.K^{-1}] are respectively the equivalent thermal conductivity and the equivalent specific heat. They depend on the moisture content in the material. Three models are thus compared. The equivalent thermal conductivity of the wet material can be expressed either by Eq. 16 or Eq. 17.

$$\lambda^* = \lambda_0(1 + \beta u) \tag{16}$$

$$\lambda^* = \lambda_{sat} + (\lambda_0 - \lambda_{sat})\frac{u_{sat} - u}{u_{sat}} \tag{17}$$

λ_0 and λ_{sat} [W.m^{-1}.K^{-1}] are respectively the dry and saturated thermal conductivity, u_{sat} [kg.kg^{-1}] the moisture content at saturation and β [-] is a fitting parameter. Contrary to β in Eq. 16, λ_{sat} can be experimentally measured.

Another relation stated in Eq. 18 is proposed in [56].

$$\lambda^* = \lambda_s^{1-n}\lambda_w^{nS_r}\lambda_a^{n(1-S_r)} \tag{18}$$

λ_s, λ_w and λ_a [W.m^{-1}.K^{-1}] respectively stand for the solid matrix, water and air thermal conductivity. S_r [-] is the degree of saturation.

The equivalent specific heat is expressed by Eq. 19.

$$c_p^* = \frac{1}{1+u}c_{p,0} + \frac{u}{1+u}c_l \tag{19}$$

with $c_{p,0}$ [J.kg^{-1}.K^{-1}] and c_l [4180 J.kg^{-1}.K^{-1}] respectively the dry specific heat of the material and the liquid water specific heat.

3. Theory

3.1. Sorption isotherms modelling

At a given temperature, starting from the dry state to the saturated state, the increase of moisture content with relative humidity allows building a so-called main adsorption curve. Conversely, starting from the saturated state to the dry state, the decrease of moisture content with relative humidity allows to build a so-called main desorption curve. These curves, defined in the standards, are the physical boundaries of the equilibrium moisture content evolution in the material. The slope of these curves defines the hygric capacity of the material, i.e. its capacity to store or release moisture.

It exists many models in literature to describe the main sorption isotherms. In this paper, the GAB (Guggenheim -Anderson - De Boer) model based on the physical sorption mechanism is used [58-61]. Its main advantage is to be able to mathematically describe the evolution of the moisture content over the whole range of relative humidity as opposed to other models like the BET, Oswin or Henderson models.

The GAB equation is described by Eq. 20:

$$\mathrm{u_j(RH)} = \frac{\mathrm{a_j b_j u_m RH}}{\left(1 - \mathrm{b_j RH}\right)\left[1 + \left(\mathrm{a_j} - 1\right)\mathrm{b_j RH}\right]}, \mathrm{j = ads\ or\ des} \tag{20}$$

where u_{ads} [kg.kg^{-1}] and u_{des} [kg.kg^{-1}] respectively represent the main adsorption and desorption isotherms, RH [%] the relative humidity. u_m [kg.kg^{-1}] is the monolayer moisture content. a_j and b_j depend on molar heat of adsorption and molar latent heat of vaporization. In practice, the parameters a_j and b_j are derived to fit experimental data. In this study, the monolayer moisture content u_m is determined from the GAB model by fitting the experimental data at low relative humidity. In theory, the GAB model, like the BET model, is physically valid only in the absence of capillary condensation, i.e. for low and medium relative humidity levels.

The monolayer moisture content u_m, which corresponds to the moisture content needed to cover the adsorbent surface by one layer of water molecules, allows to deduce the specific surface of the material. It corresponds to the total surface of the solid matrix and is expressed in Eq. 21 from the GAB fitting:

$$\mathrm{S_{GAB}} = \mathrm{S_w N_A} \frac{\mathrm{u_m}}{\mathrm{M_l}} \tag{21}$$

S_w [≈ 10 A^2] represents the surface of one adsorbed water molecule and N_A [6.02 10^{23} mol^{-1}] the Avogadro's number.

The moisture content function can also be expressed under the following form in Eq. 22:

$$u_j(RH) = \frac{u_{sat} RH(1 - b_j)[1 + (a_j - 1)b_j]}{(1 - b_j RH)[1 + (a_j - 1)b_j RH]}, j = \text{ads or des} \quad (22)$$

This relation has the advantage to be expressed in function of u_{sat}, a parameter which is experimentally characterised (cf. paragraph 2.2.1.). The parameters a_j and b_j are determined from the weighted least square method. The weighted least square estimator r shows the deviation between the experimental measurements and the predictive variable:

$$r = \sum_{i=1}^{n} p_i \left| Y_{m,i} - Y_{p,i} \right|^2 \quad (23)$$

p_i is the weight of the experimental measurements $Y_{m,i}$ and the predictive variable $Y_{p,i}$.

The adjusted coefficient of determination $\bar{R}^2$ is determined from Eq. 24:

$$\bar{R}^2 = 1 - (1 - R^2)\left(\frac{n - 1}{n - (k + 1)}\right) \quad (24)$$

with n the sample size, k the number of independent parameters and R^2 the coefficient of determination expressed in Eq. 25:

$$R^2 = 1 - \frac{\sum_{i=1}^{n} p_i \left| Y_{m,i} - Y_{p,i} \right|^2}{\sum_{i=1}^{n} \left| Y_{m,i} - \overline{Y_{m,i}} \right|^2} \quad (25)$$

The fitting quality of the GAB model is therefore tested and discussed from the evaluation of these two error indicators. The adjusted coefficient of determination gives information about the fitting ability of the model to the set of experimental data and the weighted least squares estimator about the good fit of the model.

3.2. Hysteresis modelling

In adsorption phase, an increase of the ambient relative humidity involves an increase of moisture content in the material. In desorption phase, less moisture is released from the material than moisture up taken in adsorption for a same variation of relative humidity. At a given temperature and relative humidity, the equilibrium moisture content obtained during adsorption and desorption are observed to be different. This phenomenon is known as

the hysteresis effect. Thus, the equilibrium moisture content depends not only on the relative humidity but also on the different adsorption/desorption cycles to which the material was subjected.

In this paper, the Huang model [62], which has proven its performance for different soils and construction materials [62, 63], is used to model the hysteresis phenomenon which occurs in the studied brick. According to Huang, Eqs. 26 and 27 respectively describe the adsorption and desorption scanning curves after a series of alternating processes of desorption and adsorption.

$$u(RH,i) = u_r(i) + \left(u_s(i) - u_r(i)\right)\frac{u_{ads}\,(RH)}{u_{sat}} \tag{26}$$

$$u(RH,i) = u_r(i) + \left(u_s(i) - u_r(i)\right)\frac{u_{des}\,(RH)}{u_{sat}} \tag{27}$$

The index *i* represents the number of switches between adsorption and desorption phases. The calculation of these parameters is based on the perfect closure of the scanning curves at reversal points. Scanning curve indexed *i* includes the last reversal point (RH_i,u_i) and the penultimate reversal point (RH_{i-1},u_{i-1}).

3.3. Temperature-dependence of the sorption mechanism

3.3.1. Thermodynamic model

Temperature variations can affect the evolution of moisture content inside a wall [64, 65]. The latest experimental research highlights the influence of temperature on moisture content for cement-based materials and ordinary concrete [66 - 68]. Some experimental investigations have also been performed on wood [69, 70] or on hemp concrete [71, 72].

In this paper, the effect of the temperature on moisture content relies on the thermodynamic evolution of the sorption mechanism [68]. This approach is based on the exothermic process of adsorption [73]. According to the principle of Le Chatelier and the experimental law of Van't Hoff, if the conditions of a system in equilibrium are modified, it reacts so as to oppose the changes until a new equilibrium. Thus, the exothermic nature of adsorption mechanism implies that an increase of temperature leads to a decrease of the number of adsorbed molecules and therefore the moisture content. Conversely, desorption, inverse process of adsorption, is favoured by an increase of temperature.

As presented in [68], the Clausius-Clapeyron relation is used to express the heat involved during the sorption process. The latter is called isosteric heat of sorption q_{st} [J.kg^{-1}] and is expressed in Eq. 28:

$$q_{st}(u) = -\frac{R}{M_l}\left[\frac{\partial \ln(p_v)}{\partial\left(\frac{1}{T}\right)}\right]\Bigg|_u \quad (28)$$

$p_v = RH.p_{sat}(T)$ [Pa] is the vapour partial pressure with p_{sat} [Pa] the saturated vapour pressure and T [K] the temperature. The index u means that the isosteric heat is determined at constant moisture content. The isosteric heat q_{st} is expressed from the experimental data of sorption isotherms determined at two different temperatures T_1 and T_2 by integrating Eq. (28) between two equilibrium states (T_1, $p_{v,1}$) and (T_2, $p_{v,2}$) defined for any arbitrary constant moisture content:

$$q_{st}(u) = \frac{R}{M_l}\frac{T_1 T_2}{T_2 - T_1}\ln\left[\frac{p_v(T_2, u)}{p_v(T_1, u)}\right] \quad (29)$$

The sorption isotherm at any temperature T is thus determined from an experimentally characterised sorption isotherm $RH(T_{ref}, u)$ as follows:

$$RH(T, u) = RH(T_{ref}, u)\frac{p_{sat}(T_{ref})}{p_{sat}(T)} e^{q_{st}(u)\frac{M_l(T - T_{ref})}{R\ T_{ref} T}} \quad (30)$$

The isosteric heat of sorption can also be determined from the fitting the experimental data. The model proposed by Powers and Brownyard (called PB in the rest of paper) is an example [74]:

$$q_{st}(u) = l_v + \frac{k_1}{(k_2 - u)^{k_3}} \quad (31)$$

where l_v [J.kg^{-1}] is the latent heat of condensation and k_1, k_2 and k_3 are the fitting parameters.

Another approach is to use a sorption model to represent the sorption isotherms at two different temperatures T_1 and T_2 [75]. In this paper, the GAB model is used to rely on the moisture content to the relative humidity $u = f(RH)$ at a given temperature. The inverse relation of the GAB model $RH = f^{-1}(u)$ thus allows the determination of the relative humidity at the temperatures T_1 and T_2 for a given moisture content u:

$$\begin{aligned} &\text{At } T_1, RH_1 = {f_1}^{-1}(u) \\ &\text{At } T_2, RH_2 = {f_2}^{-1}(u) \end{aligned} \quad (32)$$

The substitution of the expressions of RH_1 and RH_2 in Eq. 30 directly gives the evolution of the isosteric heat in function of the moisture content. This approach is called GAB inverse modelling (GAB IM) in the rest of the paper.

3.3.2. Physically modified GAB model

It has been previously underlined that the GAB model depends on three parameters in both traditional (Eq. 20) and modified form (Eq. 22). It is thus possible to consider the influence of temperature on sorption isotherm by modifying the expression of these parameters. The authors usually use the traditional form of the GAB to express the temperature-dependence of the parameters (u_m, a and b) [72, 76-78]. In this paper, a similar work is performed from the modified form of the GAB model (Eq. 22). The three parameters a, b and u_{sat} are expressed in function of temperature:

$$\begin{cases} u_{sat} = u_{sat,0} e^{\left(\frac{q_{sat}}{RT}\right)} \\ a = a_0 e^{\left(\frac{E_1 - E_m}{RT}\right)} \\ b = b_0 e^{\left(\frac{M_l l_v - E_m}{RT}\right)} \end{cases} \quad (33)$$

where $u_{sat,0}$, a_0, b_0 and q_{sat} are adjustable constant parameters. E_1 [J.mol^{-1}] and E_m [J.mol^{-1}] are respectively the molar heat of adsorption for one water molecular layer and the molar heat of adsorption for all water molecular layers.

From the knowledge of two sorption isotherms at two different temperatures T_1 and T_2, it is possible to identify the six unknown parameters ($u_{sat,0}$, q_{sat}, a_0, E_1, b_0, E_m) and to determine, both in adsorption and desorption, any sorption isotherm.

This physically modified model is called GAB PM in the rest of the paper.

4. Results and discussion

4.1. Physical properties

The average dry bulk density evaluated at 1848 ± 127 kg.m^{-3} and the dry bulk density of 16 raw perforated bricks are presented in Figure 4. This average value appears relevant with the data from literature even if it is slightly higher [13, 40]. A slight dispersion of the values of the 16 studied bricks has to be noted.

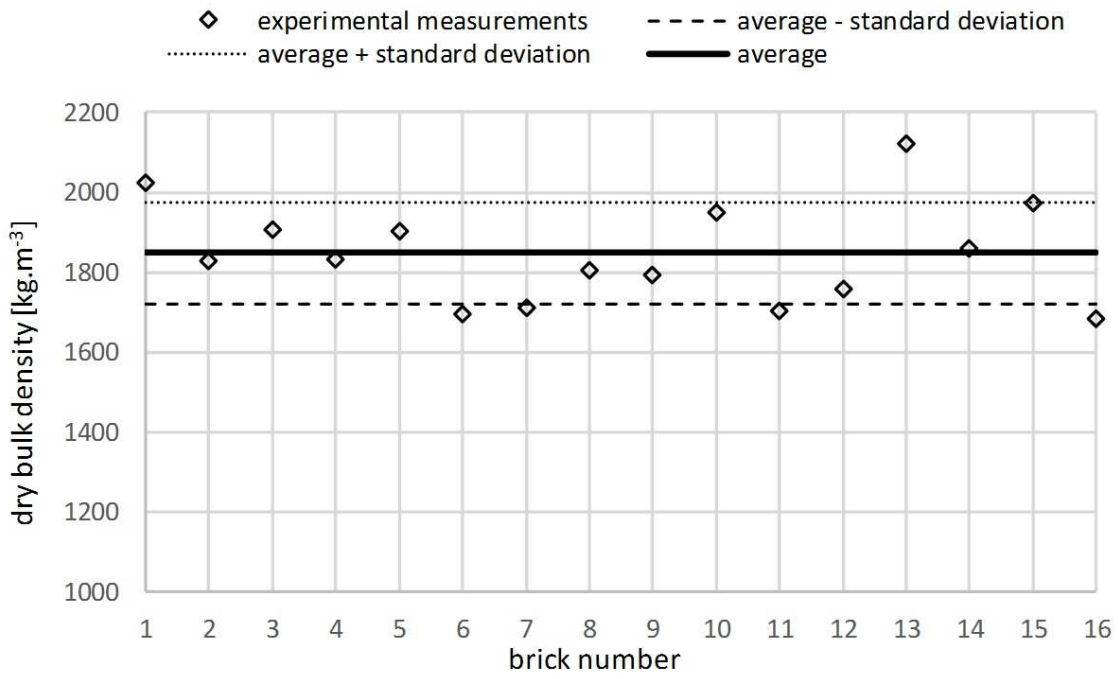

Figure 4 Dry bulk density of the raw perforated bricks

The bricks with a dry bulk density outside the standard deviation band are excluded of the study. The samples are sawed in the bricks which have a dry bulk density close to the average value.

The average dry bulk density of the prismatic samples is estimated respectively at 1866 ± 104 kg.m^{-3} and 1826 ± 92 kg.m^{-3}. The dry bulk density of these samples, which is close to the average value of the raw perforated brick, complies with the conditions defined in Eqs. 5 and 6 and is thus representative of the material.

The physical properties of the brick obtained by hydrostatic weighing method [49] are presented in Table 4.

ρ_0 [kg.m^{-3}]	u_{sat} [%]	n_0 [%]	ρ_s [kg.m^{-3}]
1826 ± 92	17 ± 2	30.6 ± 3	2631 ± 38

Table 4 Physical properties of the studied brick

4.2. Hygric properties

4.2.1. Sorption isotherms

4.2.1.1. Experimental results

Figure 5 shows the evolution of the moisture content at 10°C, 23°C and 40°C. As expected, the warmer the temperature, the lower is the equilibrium moisture content at the same relative humidity. Whatever the temperature, both main adsorption and desorption curves are very close.

At low relative humidity, from the dry state, moisture is gradually adsorbed at the level of the pore surface. The water molecules first settle into one layer (monomolecular adsorption) then, as the moisture increases, over several layers (polymolecular adsorption). Finally, from relative humidity above 90-95%RH, the phenomenon of capillary condensation appears.

Over a wide range of relative humidity until about 85%RH, it may be considered that no hysteresis occurs. This hysteresis appears for very high relative humidity over at least 85%RH.

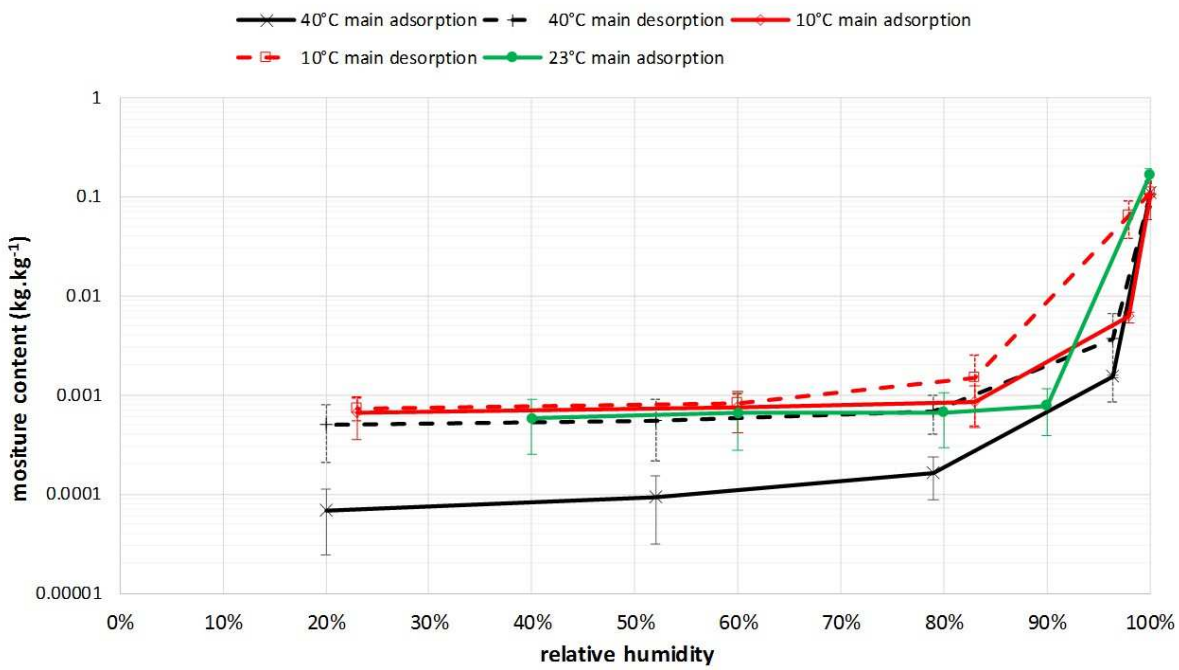

Figure 5 Experimental main adsorption and desorption isotherms at 10°C, 23°C and 40°C

The results obtained for the studied brick are compared in Figure 6 with others historical bricks presented in introduction: Vienna 1900s, Historical manufactured brick [40] and Nordic 1900s brick [13] determined at ambient temperature. The measured experimental results appear relevant with the results from the literature. The studied brick presents a hygroscopic behaviour close to that of the Historical manufactured brick.

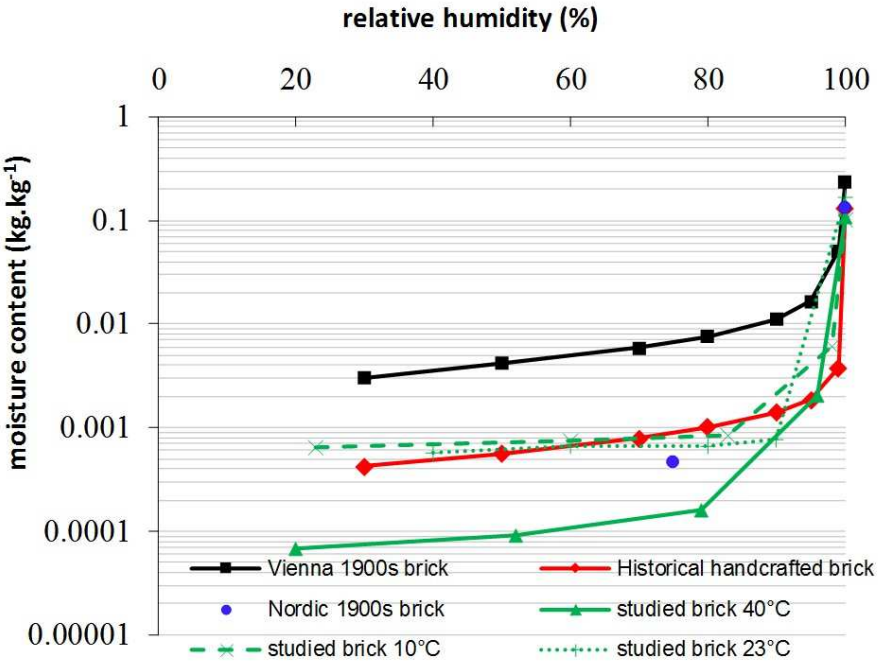

Figure 6 Main adsorption isotherms of different historical clay bricks

In order to characterize the hygroscopic behaviour of the brick, the measured sorption isotherms are compared with the results from the literature for different building materials. In Figure 7, are represented:

- the adsorption / desorption isotherm of a hemp –lime concrete (HLC) at 23°C [78]
- the adsorption / desorption isotherm of a spruce wood (SW) at 25°C [79]
- the adsorption / desorption isotherm of a hardened cement paste with W/C = 0.5 (HCP) at 25°C [40]
- the adsorption / desorption isotherm of an autoclaved aerated concrete (AAC) at 25°C [80]
- the adsorption isotherm of a limestone "Krensheimer Shelly" with a bulk density of 2440 kg.m^{-3} (LS) at 20°C [40].

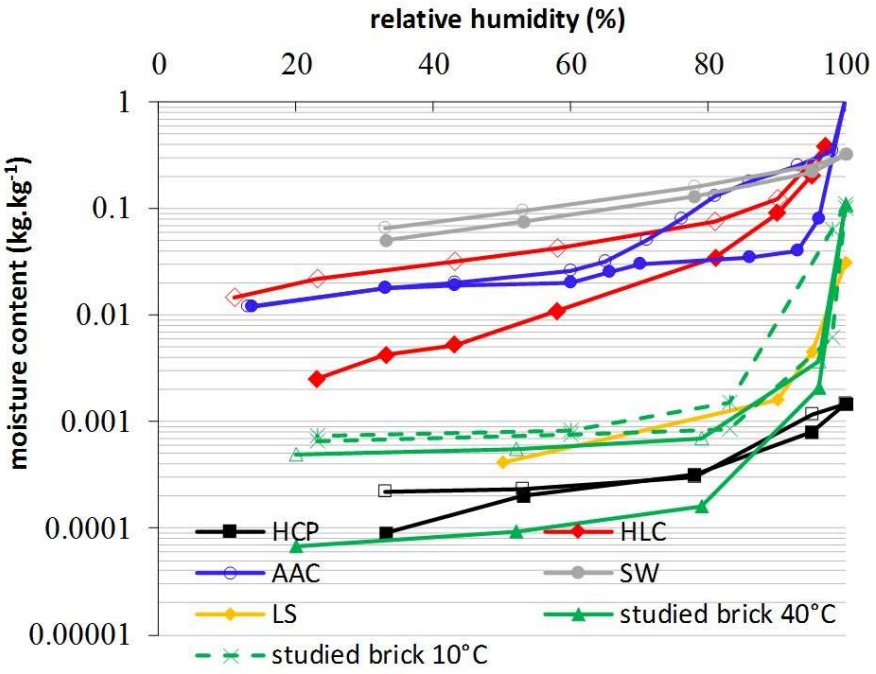

Figure 7 Main sorption isotherms of different materials used in the building sector: hemp –lime concrete (HLC) [78], spruce wood (SW) [79], hardened cement paste (HCP) [40], autoclaved aerated concrete (AAC) [80] and limestone (LS) [40]

The studied clay brick is no as hygroscopic in comparison with AAC, HLC or SW. Its hygroscopic behaviour is similar to the one of the considered LS, even though it has a higher moisture content at saturation.

4.2.1.2. Modelling of the sorption isotherms

First, only the sorption isotherms determined at 10°C and 40°C are considered. The fitted parameters and the error indicators of the GAB model are presented in Table 5 and the evolution of the sorption isotherms at 10°C and 40°C is represented in Figure 8.

If the GAB model appears suited to describe the experimental evolution of moisture content at 40°C as in adsorption as well as in desorption, it presents some limits to fit the experimental data at 10°C especially in desorption. More specifically, the form of the GAB model used in this paper and described in Eq. 22 is able to fit the experimental data at high relative humidity but fails at low relative humidity. It should be underlined that the use of the GAB model under its classical form described in Eq. 20 leads to an inverse conclusion. Indeed, as previously explained, the GAB model, is physically valid only for low and medium relative humidity levels.

Future investigations need to be done in order to find a model able to describe the isothermal evolution of the moisture content in brick under the whole range of relative humidity.

		a	b	r	$\overline{R}^2$
10°C	adsorption	102	0.9991	0.0079	0.947
	desorption	105	0.9955	0.0184	0.345
40°C	adsorption	105	0.9997	0.0024	0.986
	desorption	99	0.9991	0.0062	0.960

Table 5 Fitting parameters of the sorption isotherms at 10°C and 40°C

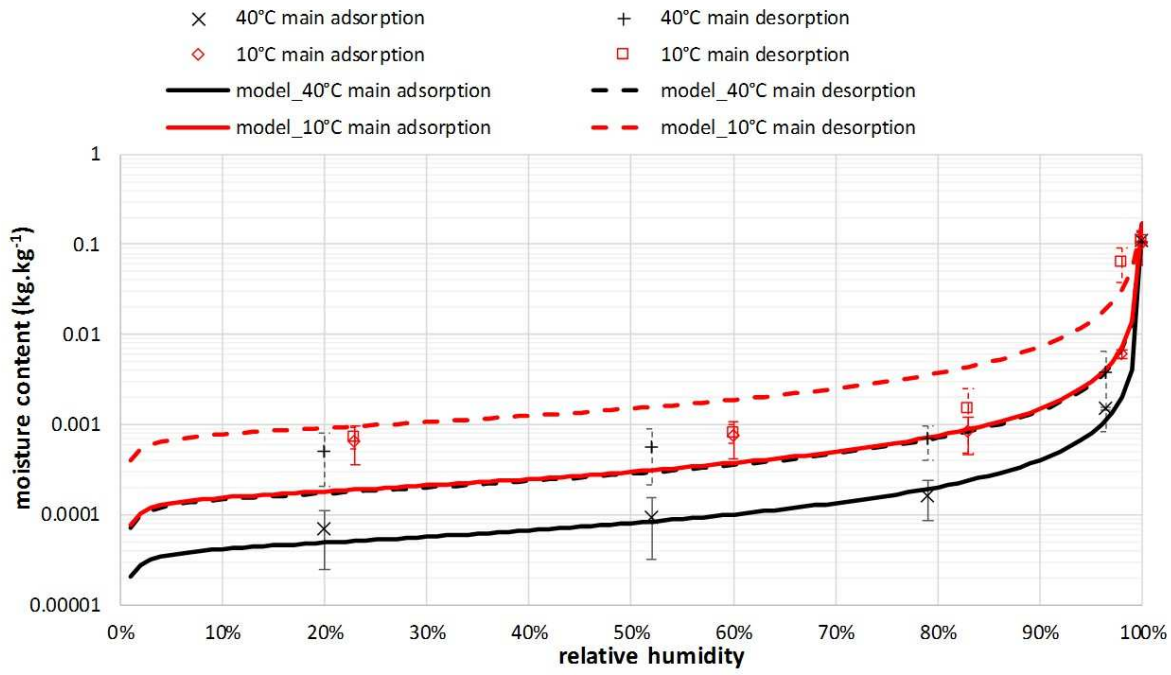

Figure 8 Experimental and modelled main adsorption and desorption curves at 10°C and 40°C

In Figure 9, the hysteresis model performance is investigated. The discrepancies observed between experimental and numerical results are explained by the fact that the GAB model under the used form in this paper fails to fit the experimental data at 10°C in desorption. However, the numerical results obtained from the Huang model chosen to represent this phenomenon are relevant to predict the evolution of the primary desorption curve 98-23%RH at 10°C in comparison with the experimental results. As experimentally highlighted, very few differences are observed between the primary desorption curve 98-23%RH and the main adsorption curve. It confirms that the hysteresis phenomenon is negligible over a very wide range of relative humidity.

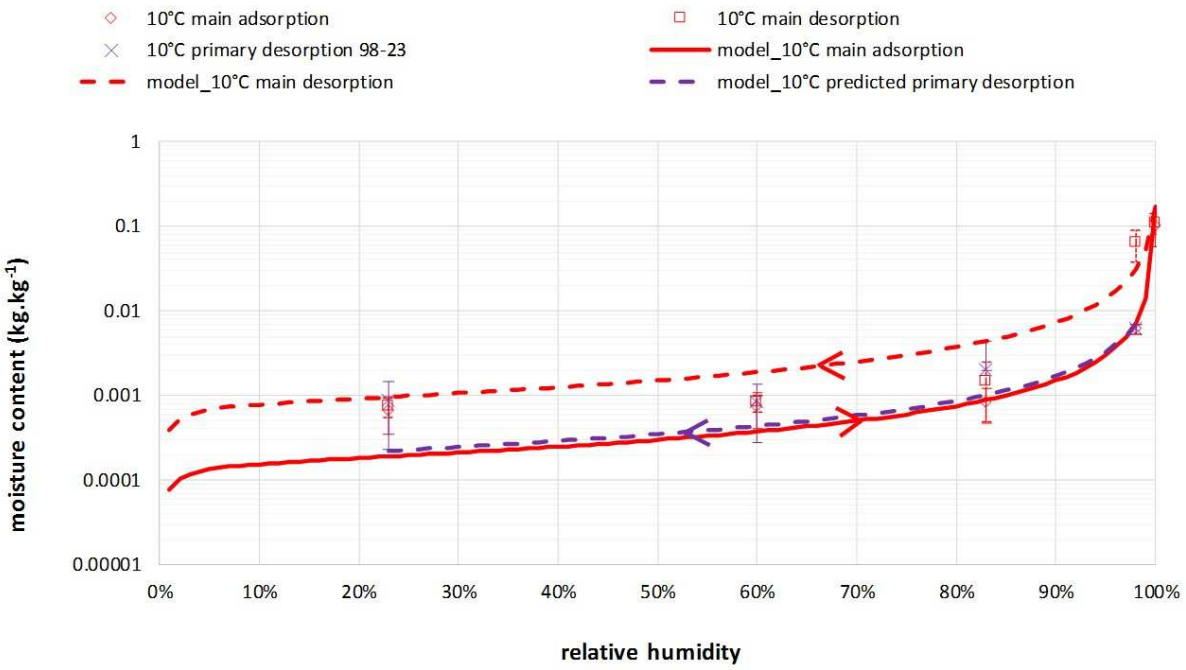

Figure 9 Experimental and modelled primary desorption curve 98-23%RH at 10°C from the Huang model [61]

The mass isosteric heat of sorption q_{st} of the studied brick is plotted on a dual scale in function of u and of the ratio u/u_m in Figure 10. Using the GAB IM model, the isosteric heat increases from the dry state to a maximal value then decreases and tends to the latent heat of condensation l_v [MJ.kg^{-1}] at a u/u_m rate around 3. This rate u/u_m is slightly lower to those found in literature for cementitious materials [68, 75] or hemp concrete [71] which are around 5. This can be explained by a specific surface of the studied brick evaluated about 20 m^2.g^{-1} at 10°C from the GAB model (Eqs. 20 and 21) in comparison with those of hemp concrete about 60 m^2.g^{-1} at 23°C and 40 m^2.g^{-1} at 30°C for concrete. One can note that because of the lack of data at low relative humidity, the estimation of the monolayer moisture content remains very rough. If possible, the determination of experimental moisture contents at low relative humidity should be encouraged for future works.

According to [72] for very low moisture contents, a first phase called chemical adsorption or chemisorption is observed. During this phase where water is chemically bound to the adsorbent (the brick) through strong interactions, the isosteric heat increases until a maximum value observed at low moisture content. This maximum corresponds to the bond energy between water molecules and the adsorbent surface created by the Van der Walls interactions. The decrease of the isosteric heat highlights the reducing influence of the adsorbent at higher moisture contents explained by an increasing distance between the water molecules and the adsorbent surface. This phase is called physical adsorption or physisorption. According to [75], the evolution of the isosteric heat is an intrinsic characteristic of the material and depends on its nature.

Contrary to the GAB IM model, no maximal value is found at low moisture contents using the PB model. The latter is suited to represent the physisorption phenomenon but fails to represent the evolution of the isosteric heat at low moisture content. The GAB IM is thus selected to model the evolution of the isosteric heat.

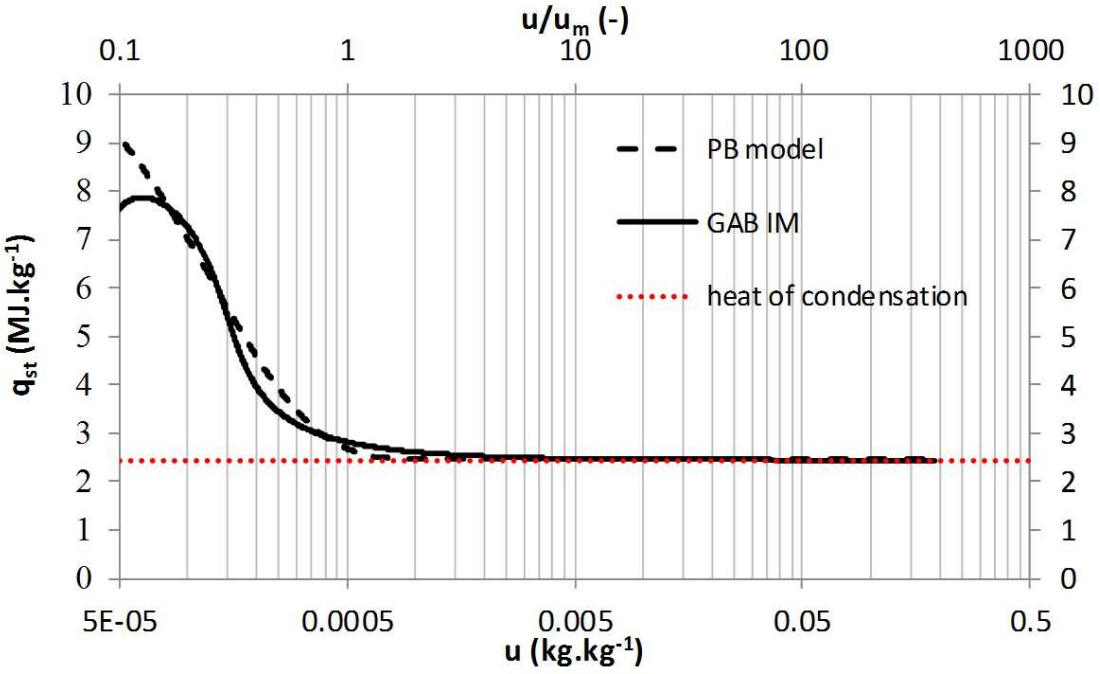

Figure 10 Evolution of the isosteric heat – The fitted parameters of PB model are k_1 = 7.5 10^3, k_2 = 1.08 and k_3 = 83.1

The GAB IM and GAB PM models used to predict the evolution of moisture content at 23°C are compared to the experimental data collected at 23°C in Figure 12.

The GAB IM and GAB PM models are close each other over a wide range of relative humidity. Nevertheless, a significant difference is observed at very high relative humidity. Indeed, the GAB PM allows reaching the moisture content at saturation whereas the GAB IM does not. This result is directly related to the mathematical formalism of the GAB IM. Indeed, the shift of the thermodynamic equilibrium leads to obtain moisture content over 100%RH which is not physically acceptable. Nevertheless, this approach could be interesting if the moisture content at saturation decreases with temperature. This has not been observed for brick over the analysed range of temperature. The GAB PM model is thus selected to predict the sorption isotherms at any temperature for the studied brick.

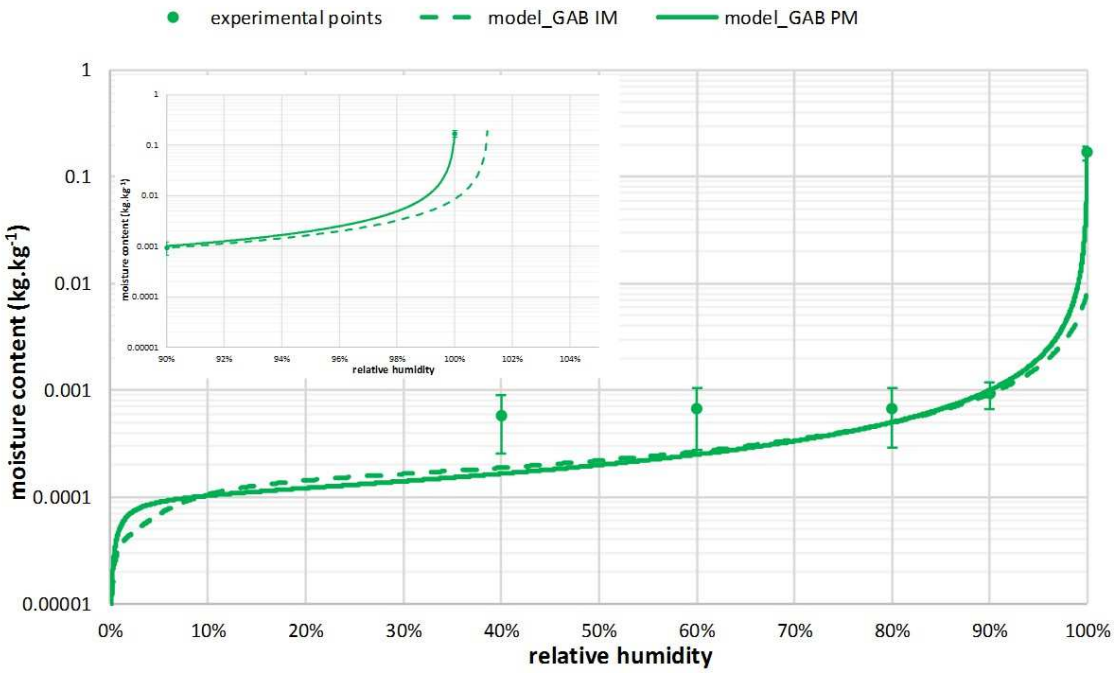

Figure 11 Comparison between the experimental data and the predictive sorption isotherm at 23°C. The figure in the top left corner is an enlargement of the curves from 90 to 105%RH

Figure 12 shows the evolution of the main adsorption and desorption curves for temperatures from 0°C to 40°C evaluated with the GAB PM model. It has to be noted that the hysteresis loop is reduced when temperature increases. In order to highlight this effect, a classical no-logarithmic scale is used in Figure 12b. This result is in accordance with the hypothesis of Ishida [80]: the increase of temperature reduces the hysteresis loop.

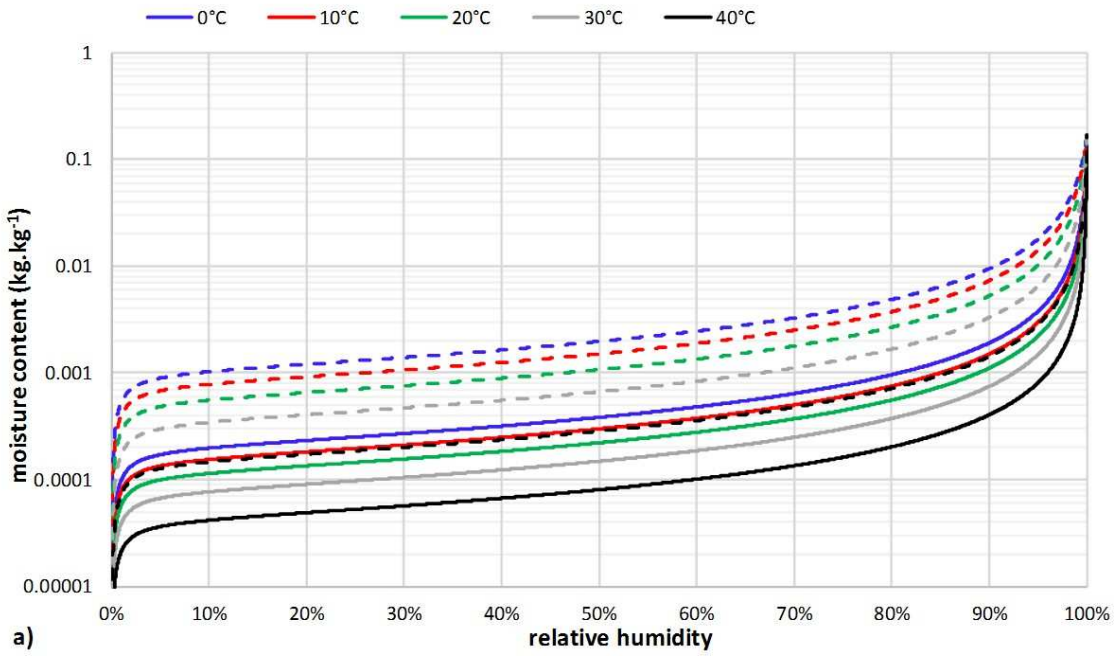

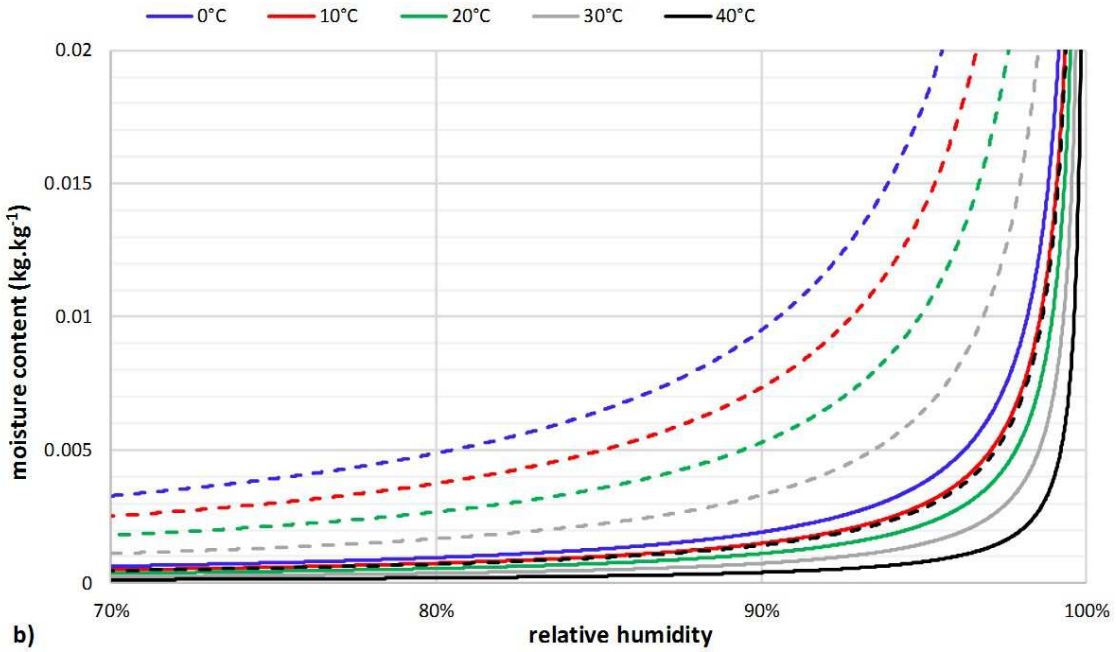

Figure 12 Predicted main adsorption and desorption curves at different temperatures – solid lines: main adsorption and dashed lines: main desorption. In Figure 12a, a semi-logarithmic scale is used and in Figure 12b a no-logarithmic scale.

4.2.2. Vapour and liquid diffusion

The samples are initially maintained at 23°C and 53%RH in a desiccator. According to NF EN 15572 [52], silica gel is used to set a relative humidity close to 0%RH and a magnesium nitrate solution to set at 53%RH. From Eq. 10, the dry vapour permeability is evaluated at 1.55 10^{-11} ± 2.5 10^{-12} kg.m^{-1}.s^{-1}.Pa^{-1}. The dry vapour diffusion resistance factor is thus about 12.6. This value appears relevant with the data from literature (cf. Table 1) The relatively high porosity gives to the studied brick a very low water vapour diffusion resistance in comparison with other structural materials.

According to the standard NF EN 15148 [53], the liquid water absorption coefficient at saturation A_w is evaluated about 0.24 ± 0.04 kg.m^{-2}.s$^{-0.5}$. This value is closed to that obtained in [13] for the Nordic 1900s brick which has a similar bulk density to the studied brick.

Figure 13 shows the evolution of the isothermal diffusion coefficients. The global evolution of the isothermal diffusion coefficients as a function of the moisture content is relevant with the theory of De Vries [81] and can be divided into three main parts. At low moisture contents, moisture is only transferred under vapour phase. The liquid condensed phase is present in adsorbed form or in capillary islands. For higher moisture contents,

capillary islands increase in size and in number. The flow section of the vapour decreases and the vapour diffuses through condensation-evaporation mechanisms at the liquid-vapour interfaces. Water in liquid phase also diffuses on the surface of the pores. At high moisture contents, as long as the continuity of the liquid phase is ensured, the transfer into the liquid phase becomes largely predominant and the isothermal liquid diffusion coefficient highly increases. It should be underlined that the liquid diffusion is negligible compared to the vapour diffusion except for very high moisture contents close to the saturation.

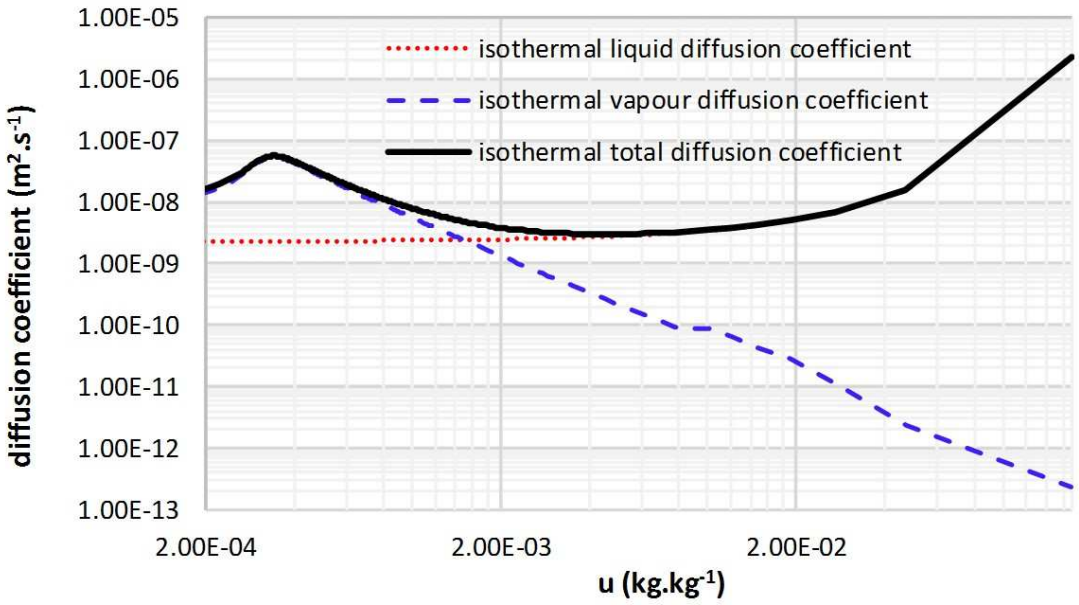

Figure 13 Evolution of the isothermal diffusion coefficient in function of moisture content

4.3. Thermal properties

The evolution of the thermal conductivity and the specific heat in function of the moisture content at 25°C are respectively represented in Figure 14a and Figure 14b. Figure 14a shows that the equivalent thermal conductivity is constant around 0.65 ± 0.01 $W.m^{-1}.K^{-1}$ for low moisture content. This means that the thermal conductivity remains constant around the dry value over a wide range of relative humidity. This result is explained on one hand by the low level of moisture content up to 90%RH and on the other hand by the fact that the dry thermal conductivity of the material and the liquid water thermal conductivity (around 0.6 $W.m^{-1}.K^{-1}$) are very close. Nevertheless, a very high thermal conductivity is measured at saturation about 1.81 ± 0.01 $W.m^{-1}.K^{-1}$. This value at saturation is three times higher than the value at dry state. Furthermore, model n°1 based on Eq. 16, model n°2

based on Eq. 17 and model n°3 based on Eq. 18 are in a good agreement with the experimental results. However, some slight differences are observed between model n°3 and the others at very high moisture content.

The dry specific heat is deduced from the equivalent value with Eq. 19 in dry state is about 616 ± 30 $J.K^{-1}.kg^{-1}$. Figure 14b shows that the specific heat over a wide range of moisture content is very close to the dry specific heat. At saturation, the specific heat capacity is estimated at 1509 ± 139 $J.K^{-1}.kg^{-1}$. The model described in Eq. 19 is in a good agreement with the experimental values except at saturation.

The measured thermal properties of the studied brick are consistent with literature data. The dry thermal conductivity of the Vienna 1900s and Historical manufactured bricks are about 0.6 $W.m^{-1}.K^{-1}$ [40]. The measured specific heat is lower than the values of the Vienna 1900s and historical manufactured bricks estimated at about 850 $J.K^{-1}.kg^{-1}$.

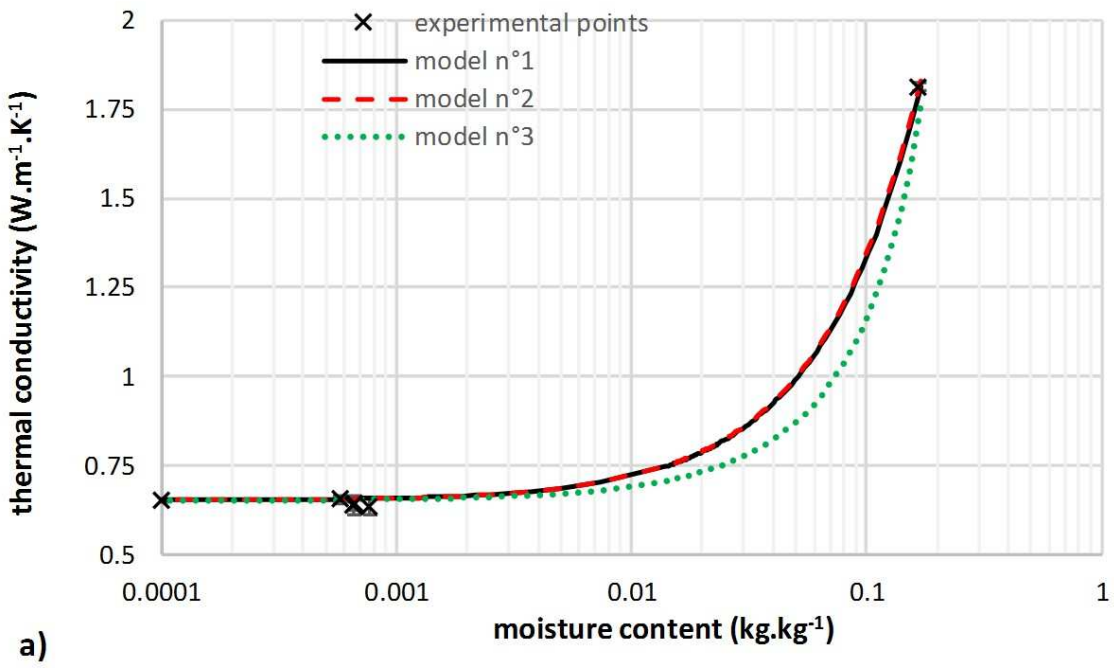

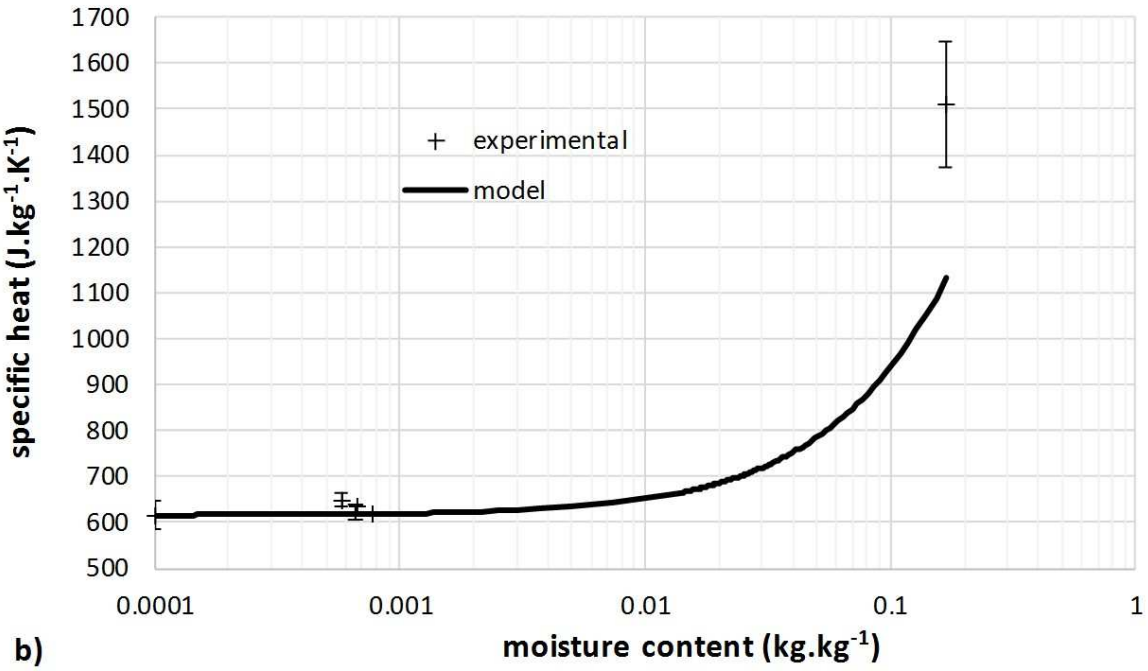

Figure 14 Evolution of the thermal conductivity a) and of the specific heat b) in function of moisture content – In order to be represented in these graphs, the thermal conductivity and specific heat at dry state are plotted for u = 0.0001 kg.kg^{-1} - The coefficient β in model n°1 based on Eq. 16 is estimated at 10.6 from the least square method.

5. Synthesis

Table 6 summarizes the main hygrothermal properties of the studied clay brick characterized in this paper in comparison with a similar heavyweight brick from the 2012 French Thermal Regulation. Despite few existing data in literature on historical fired bricks, the measured hygrothermal properties of the studied brick are in line with the scientific literature data (cf. Table 1 and Table 6*)*. Moreover, this study brings some supplementary information about the hygrothermal properties of this material, mainly its capacity to regulate moisture. This can partly be explained by its relatively high water vapour permeability. From a thermal point of view, the main interest of the studied brick concerns its high thermal effusivity and diffusivity, which results from its high density, relatively high specific heat and limited thermal conductivity. This high thermal inertia clearly contributes to the comfort of occupants and to reduce energy consumption by dampening outdoor temperature variations and storing/releasing heat. Furthermore, the studied brick presents a low hygroscopic behaviour except for very high moisture contents close to saturation.

	ρ_0	ρ_s	n_0	u_{sat}	λ_0	c_{p0}	μ_0	D_{ws}
	($kg.m^{-3}$)	($kg.m^{-3}$)	(%)	(%)	($W.m^{-1}.K^{-1}$)	($J.kg^{-1}.K^{-1}$)	(-)	(10^{-6} $m^2.s^{-1}$)
Measurements	**1826** (± 92)	**2631** (± 38)	**31** (± 3)	**17** (± 2)	**0.65** (± 0.01)	**616** (± 30)	**12.6** (± 2.0)	**2.3** (± 0.05)
2012 FTR [39]	1800 - 1900	-	-	-	0.74	1000	10	-

Table 6 Measured experimental main hygrothermal properties of the studied brick in comparison with the data of the 2012 FTR

Nevertheless, as shown in Table 6, there are significantly differences with the values given in the 2012 French Thermal Regulation [39] for a clay brick with a dry bulk density between 1800 and 1900 $kg.m^{-3}$. This can cause significant discrepancies to predict the hygrothermal response of the material subjected to climatic variations. Some future simulation works can allow to evaluate the interest to more accurately describe the hygrothermal properties of the studied historical brick, especially the thermo-dependent sorption mechanism.

6. Conclusion

This paper deals with the experimental characterization of a clay brick manufactured in the beginning of the 20th century and representative of heritage industrial buildings in eastern France. The physical and hygrothermal properties experimentally characterised in this work are also compared with theoretical models and literature data for historical bricks from the beginning of 20th century in Europe.

In this study, the standard tests for the measurement of the sorption isotherms are performed in steady state. Such tests give interesting information on the physical and hygrothermal properties but do not give information about the effective evolution of relative humidity and temperature within the material subjected to climatic variations. The measurement of the MBV (Moisture Buffer Value) according to the Nordtest protocol [83] is a way to characterize the dynamic behaviour of a material. In our opinion, it could be interesting to use and extend the Nordtest protocol to others sorption and temperature cycles. The idea is to identify the hygrothermal properties of a material solving the inverse problem with optimization techniques. The main advantage of adopting a new

protocol can be to faster characterize the hygrothermal properties of building materials than the standard time-consuming experimental methods of characterization. Moreover, this methodology has the advantage to be applied in situ. However, an accurate description of the hygrothermal transfer and mechanism is needed.

The advanced modelling of the hygrothermal properties performed in this work on the sorption mechanisms occurring in brick enables a better prediction response of a brick wall subjected to climatic variations by using a heat and moisture transfer simulation software. In addition, a better understanding of the hygrothermal behaviour of the brick could entail a better understand of its interaction with mortar joints and consequently the behaviour of the full wall. Moreover, the potential freeze-thaw damages favoured by the addition of an interior insulation layer could be better evaluated. This work is intended to be continued by numerical simulations in order to evaluate the benefit of renovation works at the wall and building scales.

These outlooks have to be investigated in future works in order to recommend suitable technological solutions to improve human hygrothermal comfort and reduce energy consumption while not creating undesirable pathologies.

Acknowledgments

This work has been supported by the EIPHI Graduate School contract ANR 17 EURE 0002 and by the French National Science Research Center (CNRS) and Region Bourgogne-Franche-Comte for its experimental part, within the frame of the projects respectively TEePI 2016-2017 and CHOB 2018-2021. The authors thank Bernard Rothlisberger, technician in the FEMTO-ST Institute, for his help in preparing the samples.

References

[1] CGDD (Commissariat Général au Développement Durable) (2018) Bilan énergétique de la France pour 2017 - Données définitives. Datalab essentiel 162. ISSN: 2557-8510.

[2] Eurostat (2019) Energy balance Sheets Data 2017. Statistical Books. DOI: 10.2785/10223.

[3] G. Piedalue, “Le patrimoine archéologique industriel du Québec”, étude produite pour le ministère de la culture, des communications et de la condition féminine, Canada, 2009.

[4] P. Prost, “Transformer et conserver”, In : cité de l’architecture et du patrimoine, Histoire et actualité du patrimoine industriel, 2012.

[5] P. Fuertes, Embodied energy policies to reuse existing buildings, Energy procedia, 115 (2017) 431-439.

[6] W.Y. Ng, C.K. Chau, New life of the building materials – recycle, reuse and recovery, Energy Procedia, 75 (2015) 2884-91.

[7] S. Lidelow, T. Orn, A. Luciani, A. Rizzo, Energy efficiency measures for heritage buildings: a literature review, Sustainable cities and societies, 45 (2018) 231-42.

[8] K. Fabbri, M. Zuppiroli, K. Ambrogio, Heritage buildings and energy performance: mapping with GIS tools, Energy and Buildings, 48 (2012) 137-45.

[9] G. Gourlis, I. Kovacic, A study on building performance analysis for energy retrofit od existing industrial facilities, Applied Energy, 184 (2016) 1389-99.

[10] M. Gasnier, Le patrimoine industriel au prisme de nouveaux défis. Usages économiques et enjeux environnementaux, Besançon : PUFC, (2018).

[11] M. Gasnier, Y. Ait Oumeziane, Les enjeux d'une recherche autour des matériaux du patrimoine industriel, Patrimoine industriel, 68 (2016) 22-25.

[12] L. Mazzarella, Energy retrofit of historic and existing buildings. The legislative regulatory point of view, Energy and Buildings, 95 (2015) 23-31.

[13] P. Johansson, S. Geving, C-E. Hagentoft, B. Petter Jelle, E. Rognvik, A. Sasic Kalagasidis, B. Time, Interior insulation retrofit of a historical brick wall using vacuum insulation panels: Hygrothermal numerical simulations and laboratory investigations, Building and Environment, 79 (2014) 31-45.

[14] P. Johansson. Tilläggsisolering av tegelfasader på flerbostadshus från 1940-till 1960-talet [Brick facade refurbishments of buildings from the 1940s to 1960s] [Thesis in swedish]. Luleå, Sweden: Luleå University of Technology, Department of Civil, Environmental and Natural Resources Engineering, 2011.

[15] C.M Capener, K. Sandin, M. Molnár, J.Jönsson. Energy efficient retrofitting of a 1950-ies multi-dwelling block house considering hygrothermal properties field measurements and simulation. In: Proceedings of 5th international building physics conference. Kyoto, Japan, May 28-31, 2012.

[16] X. Zhou, D. Derome, J. Carmeliet, Hygrothermal modeling and evaluation of freeze-thaw damage risk of masonry walls retrofitted with internal insulation, Building and environment, 125 (2017) 285-98.

[17] J.F. Straube, C.J. Schumacher. Interior insulation retrofit of load-bearing masonry walls in cold climates. Journal of Green Building. 2 (2007) 42-50.

[18] Y. Ait Oumeziane, J.P. Costes, F. El Mankibi, V. Lepiller, S. Begot, P. Desevaux. In situ monitoring of the hygrothermal behaviour of a heritage building [In French]. In: Proceedings of 28th Congrès Français de Thermique. Belfort, France, June 9-12, 2020.

[19] J. Carmeliet, D. Derome. Temperature driven inward vapor diffusion under constant and cyclic loading in small-scale wall assemblies: part 1 experimental investigation. Building and Environment 48 (2012) 48-56.

[20] J. Carmeliet J, D. Derome. Temperature driven inward vapor diffusion under constant and cyclic loading in small-scale wall assemblies: part 2 heatmoisture transport simulations. Building and Environment 47 (2012) 161-69.

[21] M. Morelli, L. Rønby, S.E. Mikkelsen, M.G. Minzari, T. Kildemoes, H.M. Tommerup. Energy retrofitting of a typical old Danish multi-family building to a "nearlyzero" energy building based on experiences from a test apartment. Energy and Building, 54 (2012) 395-406.

[22] P. Häupl, H. Fechner, H. Petzold. Interior retrofit of masonry wall to reduce energy and eliminate moisture damage: comparison of modeling and field performance. In: Proceedings of thermal performance of the exterior envelopes of whole buildings XI, Clearwater Beach, FL, USA, December 5-9, 2010.

[23] P. Mensinga, J. Straube, C. Schumacher, Assessing the freeze-thaw resistance of clay brick for interior insulation retrofit projects, In Proceedings of thermal performance of the exterior envelopes of whole buildings XI, Clearwater Beach, USA, 2010.

[24] H. Künzel, Effect of interior and exterior insulation on the hygrothermal behaviour of exposed walls. Materials and Structures, 31(2) (1998) 99-103.

[25] M. Guizzardi, D. Derome, R. Vonbank, J. Carmeliet. Hygrothermal behavior of a massive wall with interior insulation during wetting. Building and Environment, 89 (2015) 59-71

[26] B. Blocken, D. Derome, J. Carmeliet, Rainwater runoff from building facades: a review. Building and Environment, 60 (2013) 339-61.

[27] A. Kubilay, D. Derome, B. Blocken, J. Carmeliet, Numerical simulations of wind-driven rain on an array of low-rise cubic buildings and validation by field measurements. Building and Environment, 8 (2014) 283-95.

[28] T. De Mets, A. Tilmans, X. Loncour, Hygrothermal assessment of internal insulation systems of brick walls through numerical simulation and full-scale laboratory testing. Energy Procedia, 132 (2017) 753-58

[29] E. Vereecken, S. Roels, A comparison of the hygric performance of interior insulation systems: A hot box–cold box experiment**.** Energy and Buildings, 80 (2014), 37-44

[30] J. Grunewald, U. Ruisinger, and P. Haupl, The Rijksmuseum Amsterdam - hygrothermal analysis and dimensioning of thermal insulation, presented at the 3rd International Building Physics, Montreal, Quebec, Canada, 2006, 345–352.

[31] M. Harrestrup, S. Svendsen, Full-scale test of an old heritage multi-storey building undergoing energy retrofitting with focus on internal insulation and moisture. Building and Environment, 85 (2015) 123-33

[32] J. Jamal, Y. Ait Oumeziane, V. Lepiller, M. Gasnier, P. Désévaux, Simulation du comportement hygrothermique de parois de bâtiments industriels, XIIIème Colloque Inter universitaire Franco-Québécois (CIFQ), Saint-Lô, France, 2017.

[33] E. Vereecken, S. Roels. Hygric performance of a massive masonry wall: How do the mortar joints influence the moisture flux? Construction and Building Materials, 41 (2013) 697-707.

[34] X. Zhou, G. Desmarais, P. Vontobel, J. Carmeliet, D. Derome. Masonry brick-cement mortar interface resistance to water transport determined with neutron radiography and numerical modeling. Journal of Building Physics, (2020)

[35] H. Cagnon, J.E. Aubert, M. Coutand, C. Magniont, Hygrothermal properties of earth bricks, Energy and Buildings, 80 (2014) 208-17.

[36] O. Gencel, Characteristics of fired clay bricks with pumice additive, Energy and Buildings, 102 (2015) 217-24.

[37] L. Aouba, C. Bories, M. Coutand, B. Perrin, H. Lemercier, Properties of fired clay bricks with incorporated biomasses: cases of olive stone flour and wheat straw residues, Construction and Building Materials, 102 (2016) 7-13.

[38] Brick Industry Association, Manufacturing of brick. Reston, Virginia, USA: The Brick Industry Association, 2006.

[39] Th-U. Règles, Fascicule 2: Matériaux, Centre Scientifique et Technique du Bâtiment CSTB, 2017

[40] Fraunhofer IBP. WUFI Light, Vers. 6.0, Holzkirchen, Germany, 2010.

[41] P.K. Larsen, Moisture physical properties of bricks: An investigation of Falkenløwe, Stralsund and Hartmann bricks, Technical report 343, Technical University of Denmark, Department of Civil Engineering, Building Materials Laboratory, 1996.

[42] J. Kwiatkowski, M. Woloszyn, J.J. Roux, Modelling of hysteresis influence on mass transfer in building materials, Building and Environment, 44 (2009) 633-642.

[43] M. Van Belleghem, H.J. Steeman, M. Steeman, A. Janssens, M. De Paepe, Sensitivity analysis of CFD coupled non-isothermal heat and moisture modelling, Building and Environment, 45 (2010) 2485-96.

[44] X. Zhang, W. Zillig, H.M. Künzel, C. Mitterer, X. Zhang, Combined effects of sorption hysteresis and its temperature dependency on wood materials and building enclosures-part II: hygrothermal modeling, Building and Environment, 106 (2016) 181–195.

[45] B. Moujalled, Y. Ait Oumeziane, S. Moissette, M. Bart, C. Lanos, D. Samri, Experimental and numerical evaluation of the hygrothermal performance of a hemp lime concrete building: A long term case study, Building and Environment, 136 (2018) 11-27.

[46] Archives Municipales de Mulhouse : 99A760 Fonds de la Tuilerie Oscar Lesage. Procès-verbal d'essais, Laboratoire official du Syndicat des fabricants de produits céramiques de France, 24 mars 1936.

[47] Archives Municipales de Mulhouse : 99A1522 Fonds de la Tuilerie Oscar Lesage. Etudes et essais sur la variété des terres. J. Masure, Carrières et Terres, Tuileries Lesage à Mulhouse, juin 1952.

[48] NF EN ISO 12570, Hygrothermal performance of building materials and products - Determination of moisture content by drying at elevated temperature, 2000.

[49] NF EN 772-3, Methods of test for masonry units. Part 3: determination of net volume and percentage of voids of clay masonry units by hydrostatic weighing, 1999.

[50] NF EN 772-4, Methods of test for masonry units. Part 4: determination of real and bulk density and of total and open porosity for natural stone masonry units, 1999.

[51] NF EN ISO 12571, Hygrothermal Performance of Building Materials and Products – Determination of Hygroscopic Sorption Properties, 2000.

[52] NF EN ISO 12572, Hygrothermal Performance of Building Materials and Products – Determination of Water Vapour Transmission Properties, 2001.

[53] NF EN 15148, Hygrothermal performance of building materials and products e determination of water absorption coefficient by partial immersion, 2002.

[54] H.M. Künzel, Simultaneous Heat and Moisture Transport in Building Components. One- and Two-dimensional Calculation Using Simple Parameters, Fraunhofer IBP, 1995.

[55] ISO 22007–2, Plastics – determination of thermal conductivity and thermal diffusivity. Part 2: transient plane heat source (hot disc) method, 2008.

[56] S.E. Gustafsson, Transient plane source techniques for thermal conductivity and thermal diffusivity measurements of solid materials, Rev. Sci. Instrum. 62 (3) (1991) 797–804.

[57] A. Béziat, Etude expérimentale de la conductivité thermique des matériaux argileux hautement compacts : contribution à l'étude du stockage des déchets radioactifs, PhD thesis [In french], Université d'Orléans, 1987.

[58] S. Brunauer, P.H. Emmet, E. Teller, Adsorption of gases in multimolecular layers, J. Am. Chem. Soc. 60 (1938) 309–319.

[59] E.A. Guggenheim, Application of Statistical Mechanics, Clarendon Press, Oxford, 1966. Chapter 11.

[60] R.B. Anderson, Modifications of the Brunauer, Emmett and Teller, J. Am. Chem. Soc., 68 (4) (1946) 686–691.

[61] R.B. Anderson, W.K. Hall, Modifications of the Brunauer, Emmett and Teller, equation II, J. Am. Chem. Soc. 70 (5) (1948) 1727–1734.

[62] H.C. Huang, Y.C. Tan, C.W. Liu, C.H. Chen, A novel hysteresis model in unsaturated soil, Hydrological Process 19 (8) (2005) 1653–1665.

[63] Y. Aït Oumeziane, M. Bart, S. Moissette, C. Lanos, Hysteretic behaviour and moisture buffering of hemp concrete, Transp. Porous Media 103 (2014) 515–533.

[64] B. Dwi Argo, Détermination expérimentale de l'influence de l'hystérésis sur les propriétés hydriques des matériaux de Génie Civil [In French] (PhD thesis), Institut National des Sciences Appliquées de Toulouse, 1994.

[65] L. Merouani, Phénomène de sorption et de transfert d'humidité dans les bâtiments: étude expérimentale comparative d'un mortier de ciment et d'un enduit de façade [In French] (PhD thesis) Institut National Polytechnique de Grenoble, 1987.

[66] J. Hundt, H. Kantelberg, Sorptionsuntersuchungen an zemestein, zementmörtel und beton [In German], Deutscher Ausschuss für Stahlbeton Heft 297 (1978) 25–39.

[67] J.F. Daïan, Condensation and isothermal water transfer in cement mortar Part I – pore size distribution, equilibrium water condensation and imbibition, Transp. Porous Media 3 (1988) 563–589.

[68] S. Poyet, Experimental investigation of the effect of temperature on the first desorption isotherm of concrete, Cem. Concr. Res. 39 (2009) 1052–1059.

[69] P. Navi, F. Heger. Comportement thermohydromécanique du bois: applications technologiques et dans les structures [In French], PPUR Suisse, 2005.

[70] S. Merakeb, F. Dubois, C. Petit, Modélisation des hystérésis de sorption dans les matériaux hygroscopiques [In French], Comptes Rendus de Mécanique 337 (2008) 34–39.

[71] Y. Aït Oumeziane, S. Moissette, M. Bart, C. Lanos, Influence of temperature on sorption process in hemp concrete, Construct. Build. Mater. 106 (2016) 600–607.

[72] G. Promis, L. Freitas Dutra, O. Douzane, A.D. Tran Le, T. Langlet, Temperature-dependent sorption models for mass transfer throughout bio-based building materials, Construction and building materials, 197 (2019) 513-25.

[73] S. Brunauer, The adsorption of gases and vapors, Physical Adsorption, vol. I, Princeton University Press, 1945.

[74] T.C. Powers, T.L. Brownyard, Studies of the physical properties of the hardened cement paste, Portland Cement Assoc. Bull. 22 (1948).

[75] S. Poyet, S. Charles, Temperature dependence of the sorption isotherms of cemented based materials: heat of sorption and Clausius-Clapeyron formula, Cem. Concr. Res. 39 (11) (2009) 1060–1067.

[76] X. Zhang, W. Zillig, H.M. Kunzel, X. Zhang, Evaluation of moisture sorption models and modified Mualem model for prediction of desorption isotherm for wood materials, Build. Environ. 92 (2015) 387–395.

[77] R.K. Vishwakarma, U.S. Shivhare, S.K. Nanda, Moisture adsorption isotherms of guar (Cyamposis tetragonoloba) grain and guar gum splits, LWT Food Sci. Technol. 44 (2011) 969–975.

[78] F. Collet, J. Chamoin, S. Pretot, C. Lanos, Comparison of the hygric behaviour of three hemp concretes, Energy and Buildings, 62 (2013) 294-303.

[79] C. Rode, K.K. Hansen, Hysteresis and temperature dependency of moisture sorption – new measurements, 9th Nordic Symposium on Building Physics, 2 (2011).

[80] L.N. Trong, S. Asamoto, K. Matsui, Sorption isotherm and length change behaviour of autoclaved aerated concrete, Cement and Concrete Composites, 94 (2018) 136-44.

[81] T. Ishida, K. Maekawa, T. Kishi, Enhanced modeling of moisture equilibrium and transport in cementitious materials under arbitrary temperature and relative humidity history, Cement and Concrete Research, 37 (4) (2007) 565–578.

[82] D.A. De Vries, Simultaneous transfer of heat and moisture in porous media. Eos Trans AGU 39(5) (1958) 909-916.

[83] C. Rode, Moisture Buffering of Building Materials, Report BYG·DTU R-126, Technical University of Denmark (2005).